

# **Multilevel adaptive cross approximation for efficient modeling of 3D arbitrary shaped eddy current NDE problems**

Yang Bao<sup>a</sup>, Zhiwei Liu<sup>b</sup>, John R. Bowler<sup>a</sup>, and Jiming Song<sup>a\*</sup>

<sup>a</sup> Department of Electrical and Computer Engineering, Iowa State University, Ames, IA 50011, USA

<sup>b</sup> Department of Information Engineering, East China Jiaotong University, Nanchang, Jiangxi 330013, China

## **Abstract**

In this article, the multilevel adaptive cross approximation (MLACA) algorithm is presented to accelerate the boundary element method (BEM) for eddy current nondestructive evaluation (NDE) 3D problems involving arbitrary shapes. The Stratton-Chu formula, which does not have the low frequency breakdown issue, has been selected for modeling. The equivalent electric and magnetic surface currents are expanded with Rao-Wilton-Glisson (RWG) vector basis functions while the normal component of the magnetic field is expanded with pulse basis functions. The MLACA compresses the rank deficient matrices with the ACA and the butterfly algorithm. We improve the efficiency of MLACA by truncating the integral kernels after a certain distance and applying the multi-stage (level) algorithm adaptively based on the criteria for different operators to further decrease the memory and CPU time requirements while keeping almost the same accuracy comparing with the traditional MLACA. The proposed method is especially helpful to deal with the large solution domain issue of the BEM for eddy current problems. Numerical predictions are compared with the analytical, the semi-analytical predictions and the experimental results for 3D eddy current NDE problems of practical interest to demonstrate the robustness and efficiency of the proposed method.

**Keywords**—multilevel adaptive cross approximation (MLACA) algorithm, truncated integral kernels, boundary element method (BEM), eddy current testing (ECT), nondestructive testing (NDT)

\* Corresponding author email address: [jsong@iastate.edu](mailto:jsong@iastate.edu) (Jiming Song)

## 1. Introduction

Eddy current testing (ECT) is used in a variety of industries for the metal inspection due to its sensitivity, high operation speed, and repeatability. Eddy current simulation can reduce the time cost for experiment with the accurate predictions for practical nondestructive evaluation (NDE) problems. Based on these benefits, the efficient numerical simulation tools have been developed for solving ECT problems. ECT can be simulated by a variety of methods which include the analytical, the semi-analytical and the numerical methods. Analytical solutions only work for a few canonical geometries [1]. Semi-analytical methods such as the truncated region eigenfunction expansion (TREE) method [2] solve the certain structural problems in the truncated dimension with a series expansion of eigenfunctions. Numerical methods are more flexible to handle general probe flaw interaction problems. Based on the type of equations described by the problems, numerical methods can be categorized into solving the differential equations and solving the integral equations. The finite element method (FEM) which solves differential equations is popular in eddy current NDE because it is easier to implement compared with integral equation solvers [3]. However, the FEM usually consumes large computational resources due to the fact that it needs to discretize the whole solution domain with the volume meshes. The advantage of integral equation method is that the Green's function is an exact propagator that propagates a field from point A to point B, thus there is no grid dispersion error of the kind that exists in numerical differential methods where the field is propagated via a numerical grid [4]. For the integral equations method, the boundary element method (BEM) and the volume element method (VEM) have been introduced in eddy current NDE problems [5-7]. Coupled VEM-BEM has advantages for the ECT configurations involving both the narrow and volumetric flaws at the same time [8].

BEM has many advantages for solving eddy current NDE problems. One of them is that only the surfaces of considered domains need to be discretized with the result that nearly arbitrary shaped configurations can be modeled. However, for electrically large scale problems or the ones with large solution domain, the BEM leads to a huge memory requirement and computational time with an iterative

solver having a complexity  $O(N^2)$ , where  $N$  is the number of unknowns. There are a number of efficient algorithms to accelerate BEM. Among them, the multilevel fast multipole algorithm (MLFMA), which is based on the addition theorem for spherical harmonics, is one of the most efficient algorithms with the complexity  $O(N \log N)$  for both memory and computational costs [9]. However, the implementation of the MLFMA needs to deal with kernel functions of integral equations which lacks generality.

Lots of rank based methods, which have the advantage of kernel independence, have been proposed to accelerate BEM [10-14]. These methods are purely algebraic and compress the rank deficient matrices generated from the well-separated blocks. To name a few, the UV method [11], the  $H^2$ -matrix method [12], the matrix decomposition algorithm (MDA) [13] and the adaptive cross approximation (ACA) method [14]. The ACA algorithm was first proposed by Bebendorf [14] and introduced in eddy current [15-18] and extended to deal with electromagnetic compatibility related problems by Zhao *et al.* [19]. For the UV method, it needs to make the rank table first then applies it to decompress the impedance matrix. For the MDA, it generates the equivalent sources for matrix compression. While for the ACA algorithm, it is unnecessary to calculate the whole matrix. Instead, it adaptively calculates the required elements from the selected rows and columns.

Some techniques have been made to further improve the performance of ACA algorithm. Submatrices are further compressed by the QR factorization and the singular value decomposition in [20]. The sparsified ACA shows a considerable gain in efficiency over the ACA by approximating the original sub-blocks with sub-sampling of the original basis functions belonging to either subdomain [21]. The multilevel adaptive cross approximation (MLACA) is also an efficient method to compress the far block interaction matrices and has been applied to large target electromagnetic scattering problems [22-23]. In [24], the directional grouping scheme is used to further improve the efficiency of the MLACA. As with the ACA, the MLACA has the advantage such as kernel independence and is purely algebraic.

In contrast to [22-24], we apply the MLACA to the low frequency eddy current NDE problems. To the

best of our knowledge, MLACA has never been applied to low frequency eddy current problems which need to deal with both the low frequency breakdown and the large solution domain issues. Hence, one of the objectives of this paper is to report the implementations of MLACA for electrically small NDE problems. What's more, we optimize the MLACA with the integral kernel truncations and adaptively apply the multi-stage (level) algorithm based on the criteria for different operators to improve the efficiency of traditional MLACA. It is also the first time that multilevel fast algorithm shows its advantages in modeling of eddy current NDE problems.

This paper proposes MLACA to accelerate the BEM for 3D arbitrary shaped eddy current NDE problems. We select the Stratton-Chu formula to deal with the low frequency breakdown issue. Equivalent electric and magnetic surface currents and the normal component of the magnetic field are expanded by Rao-Wilton-Glisson (RWG) [25] vector basis functions and by pulse basis functions. Near and diagonal block interactions, at the finest level, need to be stored and computed as full matrices in implementing the BEM. The MLACA uses the butterfly algorithm [13] and the ACA algorithm with the truncated integral kernels after a certain distance [26-27] to approximate the well separated far block interactions. Different stages (levels) MLACA can be selected adaptively based on the criteria to approximate the far block interactions at all levels. As for the BEM modeling of eddy current NDE problems, a large solution domain is usually needed which increases the number of unknowns. MLACA with the truncated integral kernels (TMLACA) is especially useful for eddy current NDE problems with large solution domain and results in less computational cost while keeping almost the same accuracy.

The paper is organized as follows. In Section 2, a brief procedure of the Stratton-Chu formula based BEM is shown to deal with the low frequency breakdown issue. Then the details of MLACA with adaptively applying the multi-stage (level) algorithm based on criteria and the integral kernel truncations are presented in Section 3. Numerical results are compared with the analytical, the semi-analytical and the experimental results and complexity is shown for both the memory requirement and CPU time to

demonstrate the robustness and efficiency of the proposed method in Section 4. Conclusions are drawn in Section 5.

## 2. Formulation

The basic details of the formulation we use here have been given elsewhere [26-29]. For the sake of completeness, we present several key steps in our BEM. The Stratton-Chu formulas contain the surface and normal components of the surface fields [28] as follows

$$\mathbf{E}(\mathbf{r}) = \mathbf{E}^{inc}(\mathbf{r}) + i\omega\mu \oint_S G(\mathbf{r}, \mathbf{r}') \hat{\mathbf{n}} \times \mathbf{H}(\mathbf{r}') dS' + \oint_S [\hat{\mathbf{n}} \cdot \mathbf{E}(\mathbf{r}') \nabla' G(\mathbf{r}, \mathbf{r}') + \hat{\mathbf{n}} \times \mathbf{E}(\mathbf{r}') \times \nabla' G(\mathbf{r}, \mathbf{r}')] dS' \quad (1)$$

$$\mathbf{H}(\mathbf{r}) = \mathbf{H}^{inc}(\mathbf{r}) - i\omega\varepsilon \oint_S G(\mathbf{r}, \mathbf{r}') \hat{\mathbf{n}} \times \mathbf{E}(\mathbf{r}') dS' + \oint_S [\hat{\mathbf{n}} \cdot \mathbf{H}(\mathbf{r}') \nabla' G(\mathbf{r}, \mathbf{r}') + \hat{\mathbf{n}} \times \mathbf{H}(\mathbf{r}') \times \nabla' G(\mathbf{r}, \mathbf{r}')] dS' \quad (2)$$

where  $\mathbf{E}^{inc}$  and  $\mathbf{H}^{inc}$  are the incident electromagnetic fields,  $S$  is the boundary of the domain of interest,  $\mathbf{r}, \mathbf{r}' \in S$  are the field and source points respectively.  $\omega$  is the angular frequency,  $\mu, \varepsilon$  are the permeability and permittivity,  $G(\mathbf{r}, \mathbf{r}')$  is the Green function,  $\hat{\mathbf{n}}$  is the unit normal direction pointing towards solution domain,  $\nabla'$  is the gradient with respect to  $\mathbf{r}'$ . These formulas provide stable solutions at low frequencies as they remain valid even in the static limit which has no low frequency breakdown issue [29]. A low frequency approximation can be applied to (1) and (2) because the displacement currents in metal test pieces can be neglected at the frequency of ECT.

We use RWG vector basis functions [25] and pulse basis functions to expand the equivalent electric and magnetic surface currents and normal component of the magnetic field. Then we use Galerkin's method for testing. The discretized BEM matrix of the Stratton-Chu formulas reads [29]

$$\begin{bmatrix} 0.5\mathbf{T} - \mathbf{K}_1^\times & 0 & \mathbf{R}_1^\times \\ -i\mu_2/\mu_1 \mathbf{L}_2^\times & 0.5\mathbf{T} + \mathbf{K}_2^\times & 0 \\ \mu_2/\mu_1 \mathbf{K}_2^n & ik_2^2 \mathbf{L}_2^n & 0.5\mathbf{D} - \mathbf{R}_2^n \end{bmatrix} \begin{bmatrix} a \\ c' \\ d \end{bmatrix} = \begin{bmatrix} \mathbf{V}^t \\ 0 \\ 0 \end{bmatrix} \quad (3)$$

where  $k$  is the wavenumber, subscript  $i=1,2$  stand for medium 1 (air) or medium 2 (metal), the superscript  $\times$  and  $n$  denote the cross or dot products with  $\hat{\mathbf{n}}$ , and give the tangential and normal

components, respectively.  $\mathbf{D}$  is a diagonal matrix,  $\mathbf{T}$  is a diagonal-dominant sparse matrix,  $\mathbf{L}$  is the electric (magnetic) field due to the electric (magnetic) current directly,  $\mathbf{K}$  is the electric (magnetic) field due to the magnetic (electric) current, and  $\mathbf{R}$  is the electric (magnetic) field due to the electric (magnetic) charge [26]. The dimensions of each matrix are due to the numbers of basis and testing functions. The total number of unknowns is  $2N_e + N_p$ , where  $N_e$  is number of edges and  $N_p$  is number of patches. The matrix equations are solved using iterative solvers like GMRES. The preconditioners, which are detailed in [29], can be used to reduce the number of iterations.

### 3. Description of the MLACA

In this section, the MLACA with applying the multi-stage (level) algorithm adaptively based on the criteria for different operators and the truncated integral kernels is presented in details. The impedance matrix is not rank deficient as a whole. To apply the rank deficient method, a tree structure is needed to subdivide the object into blocks. The tree structure should be used to hierarchically subdivide the arbitrary shaped object into blocks, the number of blocks at the level  $l$  is increased by  $2^{l \times \text{dim}}$ , where  $\text{dim}$  is the dimension of the object. For impedance matrix as shown in (3), there are seven nonempty submatrices with different dimensions by the number of edges and patches. Two octal tree structures are used for subdivision in terms of edges and patches.

Based on the idea of the multilevel algorithm [13], the relationship between parents and children of the blocks should be recorded. For a 3D object, the octal tree is selected. A cube is used to wrap the whole object at level 0. At level 1, the cube is divided into eight smaller blocks. At level 2, each of the eight blocks is divided into eight smaller ones. This process keeps going until the smallest blocks contain the certain number of unknowns and this level is defined as the finest level. The blocks at the level  $l$  are the parents of the sub-blocks at the level  $l+1$ , while the sub-blocks at the level  $l$  are the children of the blocks at level  $l-1$ . Nonempty blocks are found by sorting at all levels. At the same level, based on the relative distance of two blocks, the block pair interactions are classified into the near-block, the diagonal-block, and

the near-far-block interactions. The near-far-block interactions are the far-block interactions for the two blocks whose parents are near-blocks. The near-far-block interaction matrices at all levels have the property of numerically low rank due to the nature of the Green function, they can be compressed by rank based methods such as the MLACA algorithm, etc. Full matrices are calculated and stored for the near and the diagonal block interactions at the finest level.

The ACA algorithm is purely algebraic and decomposes a low rank matrix arising from an asymptotically smooth function into a product of two new matrices [14-21]

$$\mathbf{Z} \approx \mathbf{U} \times \mathbf{V} \quad (4)$$

where  $\mathbf{Z}$  is a low rank matrix with dimension  $m \times n$ ,  $\mathbf{U}$  is a matrix with dimension  $m \times \text{rank}$  and  $\mathbf{V}$  is with dimension  $\text{rank} \times n$ . For the low rank matrix  $\mathbf{Z}$ ,  $\text{rank} \ll \min(m, n)$  which results in the savings. The stopping criterion is defined by  $(\|\mathbf{U}_k\| \|\mathbf{V}_k\|) / (\|\mathbf{U}_1\| \|\mathbf{V}_1\|) \leq \tau$  [30], where  $\tau$  is the tolerance,  $\|\cdot\|$  refers to the Euclidean Norm,  $\mathbf{U}_k$ ,  $\mathbf{V}_k$  stand for the row and column at  $k$ th step, respectively.

For the ACA with truncated integral kernels [26-27], because the nature of Green function is localized static field in Medium 1 and has exponential decay in Medium 2, the interaction between two far block pairs decreases as the distance between them increases. In the impedance matrix, when the diagonal block interaction is much larger than that for the far blocks, those far block interactions can be neglected. Since these interactions are trivial, this kind of truncation of kernels has almost no influence to the accuracy. This idea is practical for the problems with large solution domain in the BEM modeling for NDE problems.

The MLACA approximates the low rank matrices from the near-far-block interactions by the butterfly algorithm [13] and the ACA algorithm with the truncated integral kernels. The MLACA starts from the finest level. The program goes through all the near, diagonal, near-far-block interactions. The near and diagonal block interactions are stored by full matrices while the near-far-block interactions are approximated by 1 stage (level) MLACA algorithm based on the criteria at the finest level. Then the program goes to the parent level, certain stage (level) MLACA is properly selected based on the criteria to

approximate the near-far-block interactions at this level. The program keeps going to the coarser levels and approximates the near-far-block interactions at that level with the certain stage (level) MLACA based on the criteria until reaching the level which has no near-far-block interactions. We will show the MLACA with the truncated integral kernels first and then adaptively applying the multi-stage (level) algorithm based on the criteria for different operators will be presented.

### 3.1 MLACA with truncated integral kernels (TMLACA)

The far block pair with the binary tree structure is used to explain the details of  $S$  stage (level) MLACA with truncated integral kernels, where 1 stage (level) MLACA is the ACA algorithm.

Suppose we have an impedance matrix  $\mathbf{Z}$  for one pair of far block interaction with dimension  $m \times n$  where  $m$  and  $n$  stand for the numbers of basis functions in the observation and source blocks.  $S$  level binary tree structure is used to divide each block into two smaller ones, the relationships between parents and children are shown in Fig. 1, where the whole source or observation block is at level 1. With  $S$  level binary tree structure, the number of sub-blocks at the finest level is  $2^{(S-1)}$ . Suppose the basis functions are equally distributed into sub-blocks, each sub-block contains  $m/2^{(S-1)}$  or  $n/2^{(S-1)}$  basis functions.

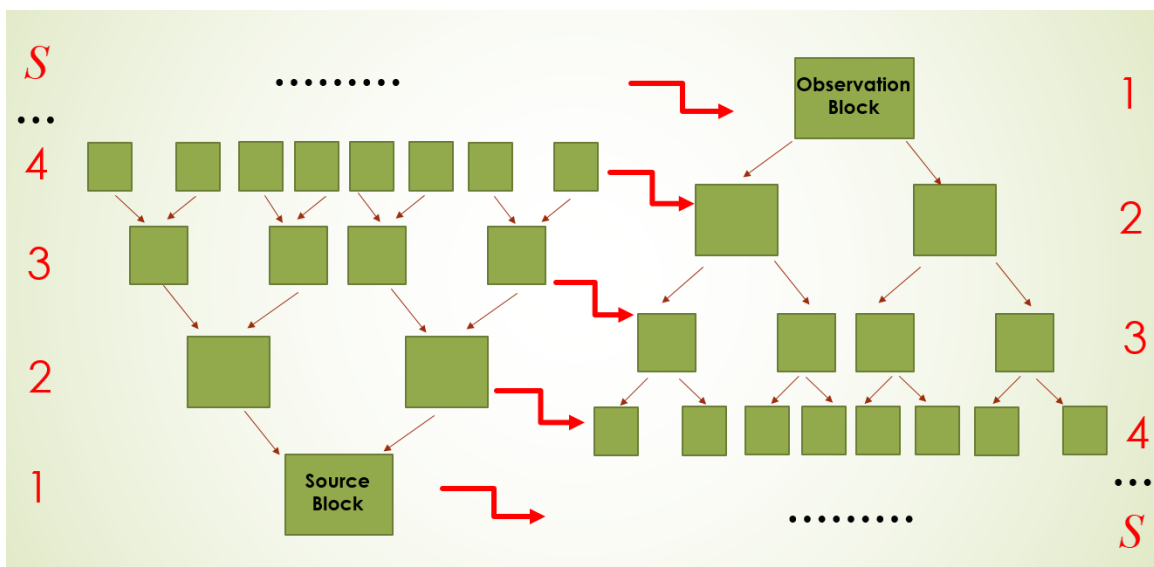


**Fig. 1.** Divide the source and observation blocks with  $S$  level binary tree structure. The multilevel

algorithm starts with the interaction between sub-blocks in the source block at level  $S$  and the observation block at level 1. Then the sub-blocks in the source block are sequentially grouped while the observation block splits.

In step 1, the multilevel algorithm starts with the interaction between sub-blocks of the source block at level  $S$  and the whole observation block as shown in Fig. 1. The impedance matrix  $\mathbf{Z}$  splits into strips and each strip stands for the interaction between the basis functions in one sub-block of the source block at level  $S$  and all the basis functions in the observation block. For traditional MLACA, each strip is approximated by the ACA algorithm. Overall, the impedance matrix  $\mathbf{Z}$  is approximated by the multiplication of two matrices  $A_0^{(1)}$  and  $B_0^{(1)}$ . The nonempty elements in  $B_0^{(1)}$  are saved and that in  $A_0^{(1)}$  are sent for compression in the next step. In this step, instead of saving  $m \times n$  elements, only  $nk$  elements in  $B_0^{(1)}$  are permanently saved [22].

While approximating each strip by ACA with the truncated integral kernels has more savings compared with the traditional MLACA. Because of the Green function decreases exponentially in the metal, some interactions between the sub-blocks in the source block at level  $S$  and the observation block can be neglected because they are much smaller than the diagonal ones. We define the threshold value for neglect as

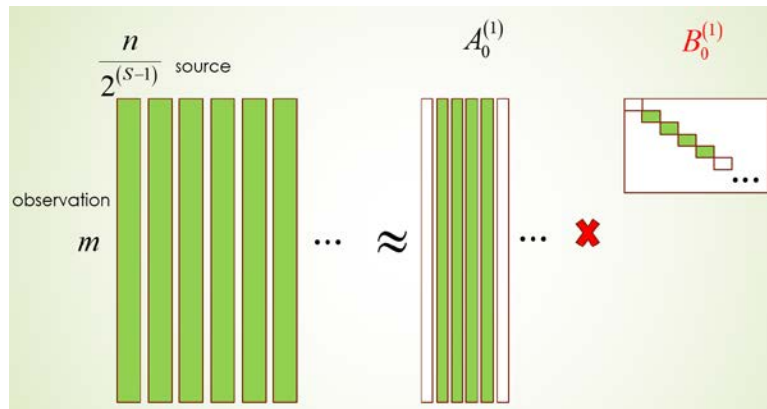
$$\Delta_1 = |Z_{mO}| / |Z_{\text{diag}}| \quad (5)$$

where  $Z_{mO}$  is the interactions between the  $m^{\text{th}}$  sub-block in the source block at level  $S$  and the observation block,  $Z_{\text{diag}}$  stands for the diagonal block interactions. By controlling the threshold value, we can decrease the storage while keeping almost the same accuracy. In Fig. 2 (a), the white strips in  $A_0^{(1)}$  and  $B_0^{(1)}$  (the interactions between the 1st and 6th sub-blocks in the source block at the level  $S$  and the observation block) can be ignored with the certain threshold value. The MLACA with truncated integral kernels leads to big storage savings in  $B_0^{(1)}$  and accelerates the matrix compression of  $A_0^{(1)}$  in the following step when the

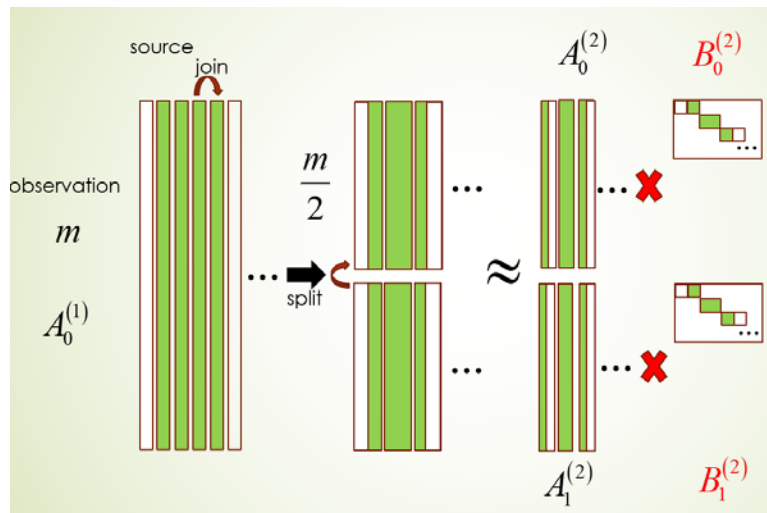
distances between the sub-blocks in the source block and the observation block are far away from each other, especially works for BEM modeling of eddy current NDE which usually requires a large solution domain.

In step 2, the  $A_0^{(1)}$  sent from step 1 goes for further decomposition. Join the contributions of the basis functions in the sub-blocks belonging to source block at level  $S$  while splitting the contributions of basis functions in the observation block. The multilevel algorithm goes to the interaction between the parents of the sub-blocks at the level  $S$  in the source block and two sub-blocks of the observation block at level 2 as shown in Fig. 1. In this step,  $A_0^{(1)}$  is approximated by four matrices:  $A_0^{(2)}, A_1^{(2)}, B_0^{(2)}, B_1^{(2)}$ , similarly, only the  $B_0^{(2)}$  and  $B_1^{(2)}$  need to be permanently stored while  $A_0^{(2)}, A_1^{(2)}$  are sent to the next step for further compression. With the help of truncated integral kernels, the storage of  $B^{(2)}$  and computational cost of  $A^{(2)}$  are less than that in the traditional MLACA.

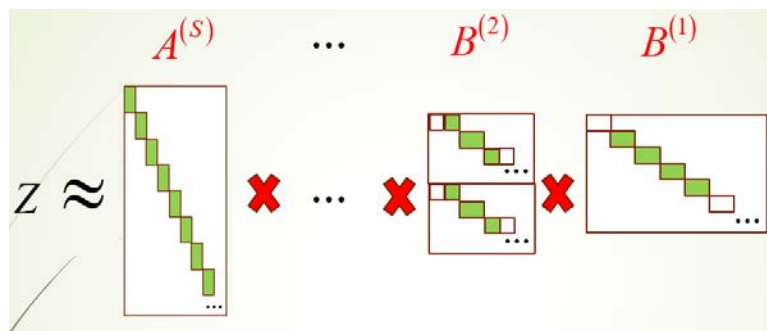
In step 3, the multilevel algorithm goes to the interaction between the parents of the sub-blocks at the level  $S-1$  in the source block and four sub-blocks of the observation block at level 3 as shown in Fig. 1. The contributions of the basis functions in the sub-blocks of the source block at the level  $S-1$  are joined while the contributions of the basis functions in the sub-blocks of the observation block at level 2 are split.  $A_0^{(2)}, A_1^{(2)}$  are compressed by eight matrices  $A_0^{(3)}, A_1^{(3)}, A_2^{(3)}, A_3^{(3)}, B_0^{(3)}, B_1^{(3)}, B_2^{(3)}, B_3^{(3)}$ .  $B^{(3)}$  need to be permanently stored and  $A^{(3)}$  are sent to the next step. Continuing this process recursively until step  $S$ . In step  $S$ , both the  $A^{(S)}$  and  $B^{(S)}$  need to be permanently stored while in other steps only the  $B$  matrices need to be stored and  $A$  matrices are sent to the next step for further compression. Finally, the original  $\mathbf{Z}$  matrix will be expressed by  $A$  and  $B$  as shown in Fig. 2 (c).



(a)



(b)



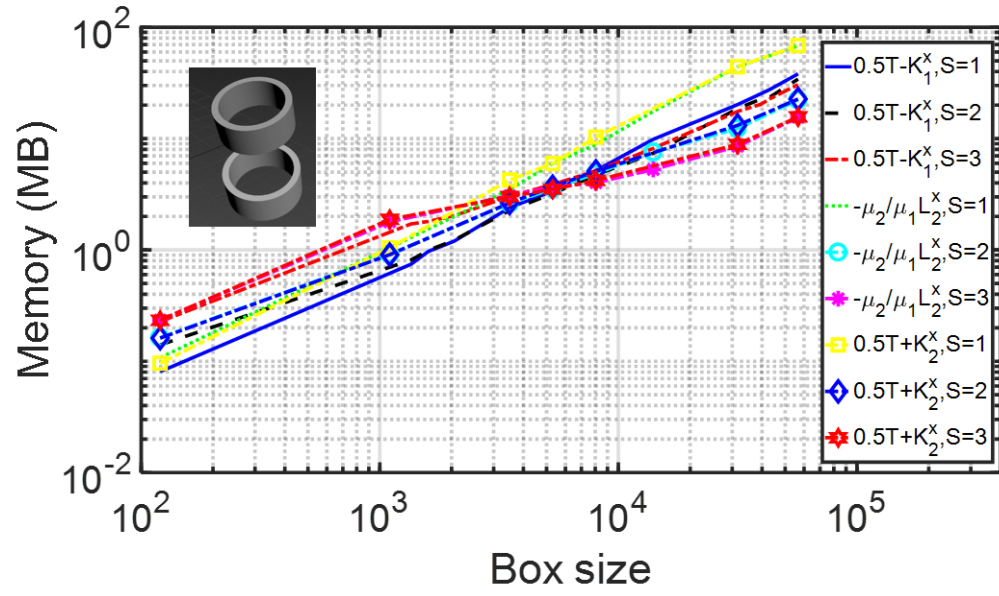
(c)

**Fig. 2.** *S* stage (level) MLACA with truncated integral kernels for matrix compression. (a) Step 1 (b) Step 2 (c) Compression for **Z** matrix. Only the green ones need to be stored and others are zero. The matrices marked in red need to be permanently stored while the ones in black don't.

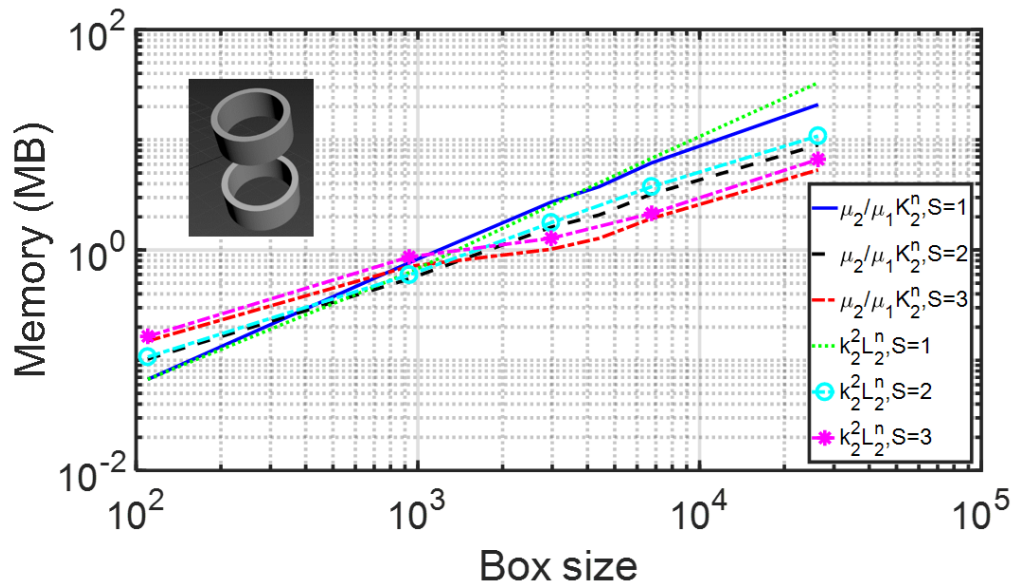
### 3.2 Adaptively apply the multi-stage (level) algorithm

In order to illustrate the method for finding the criteria for adaptively applying the multi-stage (level) algorithm for different operators, we consider a problem involving two identical coaxial conducting boreholes. Each borehole has a radius 8.32 mm, and an axial length 12 mm which is same as the axial distance between them. Keeping the edge size of the triangular mesh as one third of skin depth with the conductivity 0.84 MS/m, we vary the frequency from 3 kHz to 1.5 MHz, and accordingly the number of unknowns  $N$  per borehole changes while retaining around 83 unknowns per square skin depth. We apply the MLACA algorithm to the far block interactions between the two boreholes. Fig. 3 (a) shows the memory requirement of MLACA algorithm for  $0.5\mathbf{T}-\mathbf{K}_1^\times$ ,  $-i\mu_2/\mu_1\mathbf{L}_2^\times$ ,  $0.5\mathbf{T}+\mathbf{K}_2^\times$  operators with matrices' dimension  $N_e$  by  $N_e$  when the ACA tolerance  $\tau$  is  $10^{-3}$ .

From Fig. 3 (a), we can observe that for the operator  $0.5\mathbf{T}-\mathbf{K}_1^\times$ , 1 stage (level) MLACA is most efficient when box size is smaller than around 3000, 2 stage (level) MLACA is the most efficient one when the box size is between around 3000 and 23000, after that, 3 stage (level) MLACA shows the advantages over others. Similarly, we can conclude the criteria for  $-i\mu_2/\mu_1\mathbf{L}_2^\times$  and  $0.5\mathbf{T}+\mathbf{K}_2^\times$  operators.



(a)



(b)

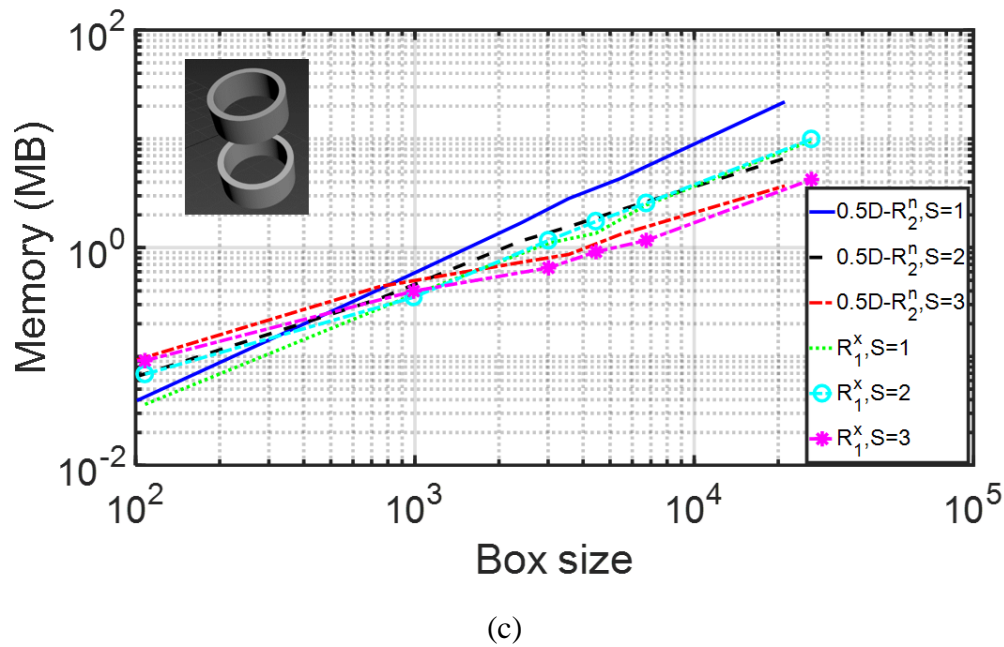


**Fig. 3.** Memory requirement of the far block interactions for a pair of boreholes. Varying frequency with a fixed mesh density and object, accordingly the number of unknowns in each borehole changes. (a) Matrices of three operators with dimension  $N_e$  by  $N_e$ . (b) Matrices of two operators with dimension  $N_p$  by  $N_e$ . (c) Matrices of two operators with dimension  $N_e$  by  $N_p$  and  $N_p$  by  $N_p$ , respectively.

In Fig. 3 (b), we show the memory requirement of the MLACA algorithm for  $\mu_2/\mu_1 \mathbf{K}_2^n$ ,  $ik_2^2 \mathbf{L}_2^n$  operators which are with matrices' dimension  $N_p$  by  $N_e$ . For  $\mu_2/\mu_1 \mathbf{K}_2^n$  operator, 1 stage (level) MLACA is most efficient when the box size is smaller than around 340. With the box size between around 340 and 1500, 2 stage (level) MLACA should be used and 3 stage (level) MLACA should be considered with the box size larger than around 1500. The criteria for the  $ik_2^2 \mathbf{L}_2^n$  operator can be determined in a similar way.

Fig. 3 (c) shows the memory requirement of the  $0.5\mathbf{D}-\mathbf{R}_2^n$  and  $\mathbf{R}_1^x$  operators which are with matrices' dimensions  $N_p$  by  $N_p$  and  $N_e$  by  $N_p$ , respectively. 1 stage (level) MLACA shows the advantage when the box size is smaller than around 350, 2 stage (level) MLACA seems to be more efficient with the box size between around 350 and 1000. When the box size is larger than 1000, 3 stage (level) MLACA should

be used. The criteria for the  $\mathbf{R}_1^\times$  operator can be determined in the same way.

Almost the same criteria are observed for all the operators when the frequency is fixed, vary the mesh density, and accordingly the number of unknowns per borehole changes. Once we know the criteria for each operator, we can decide which stage (level) MLACA should be used for near-far-block interactions of the certain level considering about the box size. Adaptively applying MLACA can improve the performance most.

Next, we are going to show the advantages of adaptively controlling multi-stage (level) algorithm based on the criteria adopted. A borehole is used with radius 8.32 mm and height 48 mm. The frequency is 30 kHz. The number of unknowns are increased by around factor four with changing the mesh density. The octal tree is used to divide the object hierarchically until the box size at the finest level is around 40 with the number of levels ranges from 3 to 7 for different numbers of unknowns. Different combinations of 1, 2 and 3 stages (levels) MLACA are selected with tolerance  $\tau$  equals  $10^{-3}$  for level ranges from 1 to 3. When the level is over 3, 1 stage (level) MLACA should be used based on the criteria. Table I shows the memory requirement of the top three levels with different stages (levels) MLACA for the  $0.5\mathbf{T}-\mathbf{K}_1^\times$  operator. In Table I,  $S=X/Y/Z$  represents X stage (level) MLACA is applied for the near-far-block interactions at level 3, Y stage (level) MLACA is applied for the near-far-block interactions at level 2 and Z stage (level) MLACA is applied for the near-far-block interactions at level 1.

**TABLE I**  
TOTAL MEMORY REQUIREMENT (GB) OF THE TOP THREE LEVELS WITH  
DIFFERENT STAGES (LEVELS) MLACA FOR  $0.5\mathbf{T}-\mathbf{K}_1^\times$  OPERATOR

Number of unknowns	$S=1/1/1$	$S=1/2/3$	$S=1/2/2$	$S=1/1/3$	$S=1/1/2$
3252	0.0631	0.0870	0.0791	0.0718	0.0639
13075	0.270	0.295	0.284	0.279	0.268
54456	1.04	1.20	1.18	1.01	0.994
219816	4.89	4.41	4.42	4.67	4.69
888376	19.9	18.0	18.7	18.8	19.1

When the number of unknowns is 3252, the number of levels is 3. The box size at level 1 is around 800,

at level 2 is around 200 and at level 3 is around 50. Based on the criteria concluded from Fig. 3 (a), 1 stage (level) MLACA should be applied to the near-far-block interactions at the levels from 3 to 1 ( $S=1/1/1$ ) to optimize the performance which is shown in Table I. Assigning  $S=1/1/1$  results in the use of 1% memory less than  $S=1/1/2$ , 12% memory less than  $S=1/1/3$ , 20% memory less than  $S=1/2/2$  and 27% memory less than  $S=1/2/3$ . With the criteria, at most 27% memory saving could be achieved.

When the number of unknowns is 13075, the number of levels is 4. The box size at level 1 is around 3200, at level 2 is around 800 and at level 3 is around 200, based on the criteria concluded,  $S=1/1/2$  should be the most efficient one. From Table I, we can observe that for the memory cost at the levels from 3 to 1,  $S=1/1/2$  uses 1% memory less than  $S=1/1/1$ , 4% memory less than  $S=1/1/3$ , 6% memory less than  $S=1/2/2$  and 9% memory less than  $S=1/2/3$ .

When the number of unknowns is 54456, the number of levels is 5. The box size at level 1 is around 13000, at level 2 is around 2900 and at level 3 is around 800, based on the criteria we concluded, again  $S=1/1/2$  should be the most efficient one. From Table I, for the memory cost of 3 to 1 levels,  $S=1/1/2$  uses 4% memory less than  $S=1/1/1$ , 2% memory less than  $S=1/1/3$ , 16% memory less than  $S=1/2/2$  and 17% memory less than  $S=1/2/3$ .

For the other two numbers of unknowns, a similar test is done: increase the number of levels to keep the box size at the finest level around 40. The memory savings for the most efficient and the least one are 11% and 10%, respectively. Overall, the criteria work well for cases shown above. Basing on the criteria of the  $0.5\mathbf{T}-\mathbf{K}_1^\times$  operator, we can adaptively apply the MLACA to optimize the performance. We also do this test for other operators and the criteria work well for all of them. We tested the far block interactions of two spheres and plates with retaining the number of unknowns per square skin depth at each frequency. The criteria for all other operators are similar to the ones we found and will be regarded as the reference. By adaptively applying the multi-stage (level) algorithm based on the criteria, we can optimize the overall performance of MLACA.

## 4. Numerical Results

In this section, the MLACA with the truncated integral kernels (TMLACA) is applied to accelerate the BEM modeling for 3D arbitrary shaped eddy current NDE problems adaptively based on the criteria. Several eddy current NDE cases are presented. Impedance changes are calculated by the Auld's formulation [31]. Numerical predictions calculated from the MLACA based BEM and the TMLACA based BEM are compared with the analytical, the semi-analytical, the BEM and the ACA based BEM predictions and the experimental results to show the accuracy of the proposed model. The complexity of MLACA is provided to show the efficiency. Generalized minimal residual (GMRES) is selected as an iterative solver with the relative residual error  $10^{-3}$ . All the computations are done on Intel Xeon Workstation at 2.6 GHz in double precision.

### 4.1 Accuracy

The number of unknowns depends on the mesh density. In the BEM for wave interactions, 10 to 20 unknowns per wavelength are used [9]. However, for eddy current problems in highly conductive metals, 2 to 4 unknowns per skin depth give similar order of accuracy. The first case is a plate problem with the coil placed above it as shown in Fig. 4. The coil impedance changes due to the nonmagnetic conductor plate and ferromagnetic steel plate are calculated. For the nonmagnetic conductor plate, two kinds of materials regarding two detecting coils which operate at different frequencies are shown. The parameters of the coil, nonmagnetic conductor and the incident fields from a coil with rectangular cross section can be found in [2].

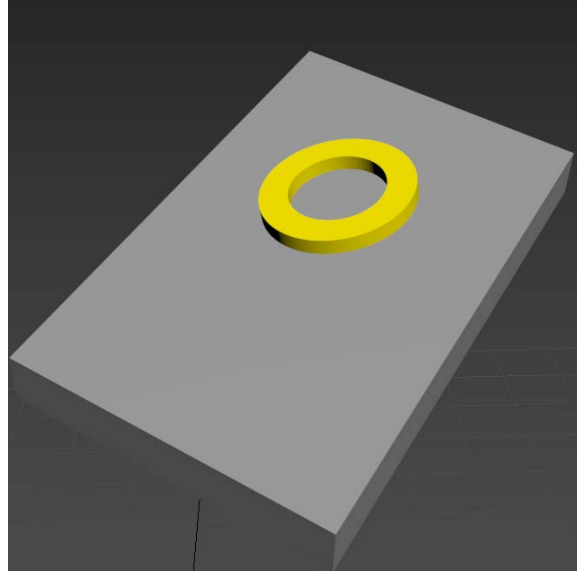


**Fig. 4.** Coil above the plate.

For both cases, the tolerance of MLACA is  $\varepsilon = 10^{-3}$  and the threshold value  $\Delta_l$  of TMLACA is  $10^{-4}$ . For the case with placing coil C5 above block B1 which operates at 850 kHz, the solution domain is 120 mm by 120 mm, the skin depth is 3.42 mm, and the mesh size is 3.21 mm with the number of unknowns 15,024. The number of levels is 3 (level 0, 1, 2 and 3) with the box size for edges around 1500 at level 1, around 360 at level 2 and around 90 at level 3, and for patches around 1000 at level 1, around 250 at level 2 and around 60 at level 3. There are no near-far-block interactions at level 1. Based on the criteria, we adaptively apply 1 and 2 stages MLACA to different operators at different levels for the problem.

Table II shows the memory requirement, CPU time and the good agreements in both the real and imaginary parts of impedance changes achieved by the experiment, the analytical method, the semi-analytical method, the BEM, the ACA based BEM, the MLACA based BEM and the TMLACA based BEM for placing coil C5 above block B1. The relative differences between those methods are smaller than 1%. One point should be drew attention is that many entries of the matrix blocks from the  $\mathbf{K}$  operator are naturally null for the plate shape problems. This is because the testing and basis patches are co-planar. MLACA algorithm can still work for other non-zero matrices which leads to good accuracy as shown in

Table II.

For the performance of the case of coil C5, the relative differences for the impedance changes determined from the experiment, the analytical method, the semi-analytical method, the BEM, the ACA based BEM, the MLACA based BEM and the TMLACA based BEM are smaller than 1%. MLACA based BEM only needs 13% memory of the BEM and uses 10% memory less than the ACA based BEM. The memory cost for the far block interactions and CPU time per iteration of the TMLACA based BEM are 71% and 26% less than the MLACA based BEM, respectively. Overall, the TMLACA based BEM needs 10% memory of BEM and uses 20% memory less than the MLACA based BEM.

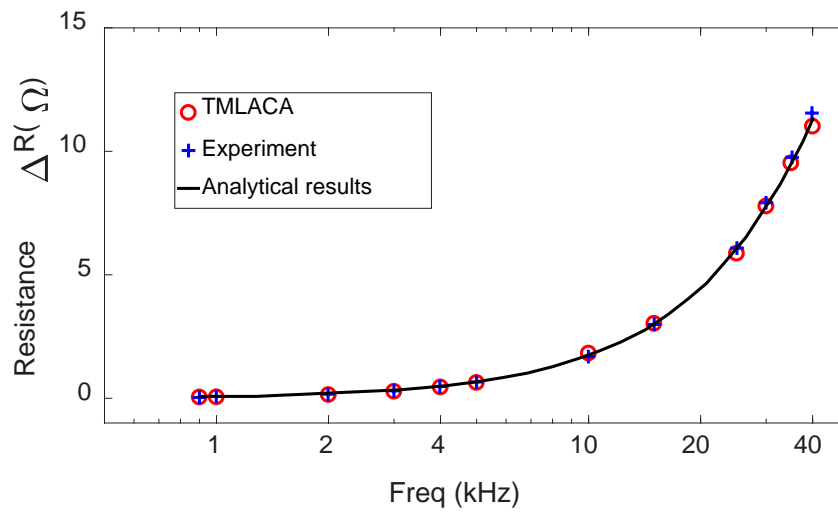
**TABLE II**  
 COIL C5 IS ABOVE THE BLOCK B1

	IMPEDANCE CHANGE ( $\Omega$ )	FAR BLOCK INTERACTION MEMORY REQUIREMENT (MB)	MEMORY REQUIREMENT (MB)	CPU TIME PER ITERATION (s)
BEM [27]	22.1529 + 70.4094i	n/a	3444.2	0.62
ACA [27]	22.1529 + 70.4094i	171.27	490.1	0.172
MLACA	22.1529 + 70.4094i	121.27	440.1	0.156
TMLACA	22.1906 + 70.4197i	35.21	354.0	0.116
Experiment [2]	20.00 + 70.5i	n/a	n/a	n/a
Dodd & Deeds [1]	22.20 + 70.49i	n/a	n/a	n/a
Theodoulidis & Bowler [2]	22.25 + 70.45i	n/a	n/a	n/a

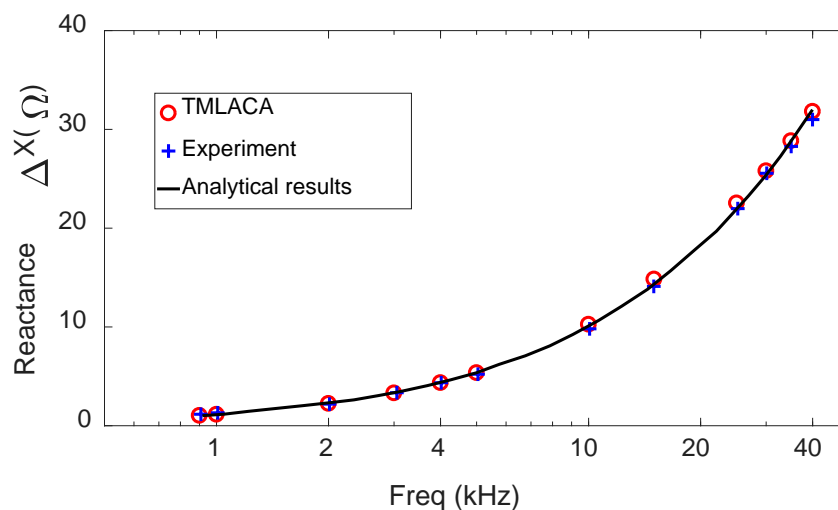
As to the case with coil C27, the MLACA based BEM only needs 11% memory of the BEM. For the memory cost of the far block interactions, the MLACA based BEM uses 18% less than the ACA based BEM while the TMLACA based BEM uses 44% less than the MLACA based BEM. Overall, the TMLACA based BEM needs 10% memory of the BEM and uses 7% memory less than the MLACA based BEM. For the CPU time per iteration, the MLACA based BEM only needs 19% of the BEM and the TMLACA based BEM uses 9% less than the MLACA based BEM.

Our method also works well for a problem in which the impedance of a coil above a ferromagnetic plate is determined. A set of parameters related to this problem is given in [32]. The TMLACA method shows

the good agreements for the changes of resistance and reactance with frequency, compared with the experimental and the analytical methods [32] as shown in Fig. 5. The skin depth varies from 0.25 mm to 1.7 mm for different frequencies. The solution domain is about 20 times the skin depth and edge size of the triangular mesh is about two third of the skin depth at each frequency. 1 and 2 stages MLACA are adaptively used based on the criteria, the tolerance  $\tau$  is  $\varepsilon=10^{-3}$  and the threshold value  $\Delta_1$  of the TMLACA is  $10^{-4}$ .



(a)



(b)

**Fig. 5.** The (a) resistance and (b) reactance changes of a circular coil above a flawless 440SS slab as a function of frequency. The results achieved by the TMLACA based BEM, the experiment and the analytical method [32] are compared.

The second case concerns a coil with the finite cross section placed inside the borehole as shown in Fig. 6. In eddy current NDE, the modeling of the coil placed inside the cylindrical structures such as tubes or boreholes is a very interesting topic in considering of thousands of tubes are used in the heat exchangers and the steam generators to increase the amount of heat transferred. The MLACA is applied to evaluate the impedance changes when the coil, whose axis is the same as that of a borehole, places in an Inconel 600 borehole with conductivity 0.84 MS/m. The parameters of this case are in [33].

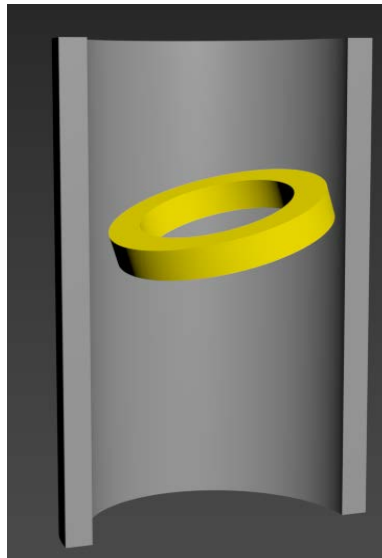


**Fig. 6.** Coil inside the borehole.

The impedance changes calculated by the semi-analytical method, the BEM, the ACA based BEM, the MLACA based BEM and the TMLACA based BEM are shown in Table III. Two frequencies at 30 kHz and 50 kHz are selected to demonstrate the accuracy and efficiency of the MLACA, the details of the mesh are shown in Table III. For frequency at 30 kHz, the number of levels is 3 with the box size for edges

around 800 at level 2 and around 100 at level 3, and for patches around 550 at level 2 and around 70 at level 3. For frequency at 50 kHz, the number of levels is 3 with the box size for edges around 1200 at level 2 and around 150 at level 3, and for patches around 770 at level 2 and around 100 at level 3. 1 and 2 stages MLACA are used for the operators at different levels based on the criteria. The tolerance for the MLACA is  $\varepsilon = 10^{-3}$  and the threshold value  $\Delta_1$  of the TMLACA is  $10^{-4}$ .

**TABLE III**  
 COIL INSIDE A BOREHOLE

	30 kHz	50 kHz
Skin depth (mm)	3.2	2.5
Truncated height (mm)	48	37.5
Mesh size (mm)	0.800	0.625
Number of unknowns	34,912	49,152
Impedance change ( $\mathbf{m}\Omega$ )		
Wu & Bowler [33]	9.421+18.58i	8.873+21.95i
BEM [27]	9.483+18.76i	8.862+21.96i
ACA [27]	9.482+18.76i	8.862+21.96i
MLACA	9.482+18.76i	8.862+21.96i
TMLACA	9.518+18.64i	8.890+21.95i

From Table III, the good agreements can be observed for both real and imaginary parts of impedance changes calculated by the semi-analytical method, the BEM, the ACA based BEM, the MLACA based BEM and the TMLACA based BEM. The relative differences are smaller than 1%. At 30 kHz and 50 kHz, MLACA based BEM only needs 19% and 15% memory of BEM, respectively. At 30 kHz, the TMLACA based BEM uses 56% less memory in the far block interactions and 32% less CPU time per iteration than the MLACA based BEM, while at 50 kHz the corresponding reduction is 40% and 23%. At 30 kHz, the relative differences of impedance changes between the BEM and the TMLACA based BEM in the real and imaginary parts are 0.37% and 0.64%, while that at 50 kHz are 0.32% and 0.046%, respectively.

The third case considered is that of a single turn coil symmetrically located above a conducting sphere as shown in Fig. 7. The incident electromagnetic field by a single turn coil is in [34]. We consider the case that the excitation frequency is 10 kHz, the radius of single turn coil  $r_c$  is 0.1 m, the radius of the

conducting sphere  $\rho_1$  is 0.1 m, and the axial distance between the coil and the surface of the sphere  $h$  is 0.01 m.  $\beta = \sqrt{2}r_c/\delta$  is 10 with the skin depth  $\delta$  is 0.014 m, the conductivity is 0.13 MS/m and the relative permeability is 1. Table IV shows the memory requirement, the CPU time and the impedance changes achieved by the analytical method, the BEM, the ACA based BEM, the MLACA based BEM and the TMLACA based BEM. The edge size of the triangular mesh is about two third of the skin depth. The number of unknowns is 13,544. The tolerance for the MLACA is  $\varepsilon = 10^{-3}$  and the threshold value  $\Delta_1$  of the TMLACA is  $10^{-4}$ . The number of levels is 3 with the box size for edges around 640 at level 2 and around 90 at level 3, and for patches around 430 at level 2 and around 60 at level 3. Based on the criteria, we adaptively apply 1 and 2 stages MLACA to different operators at different levels.

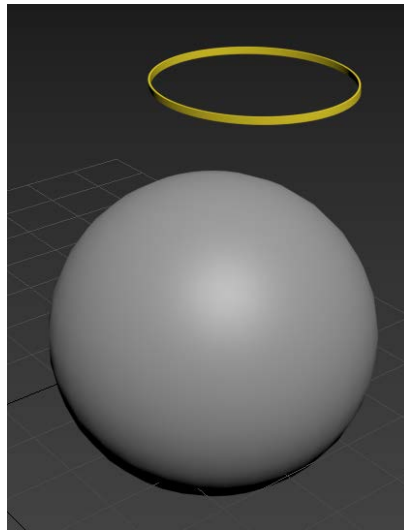


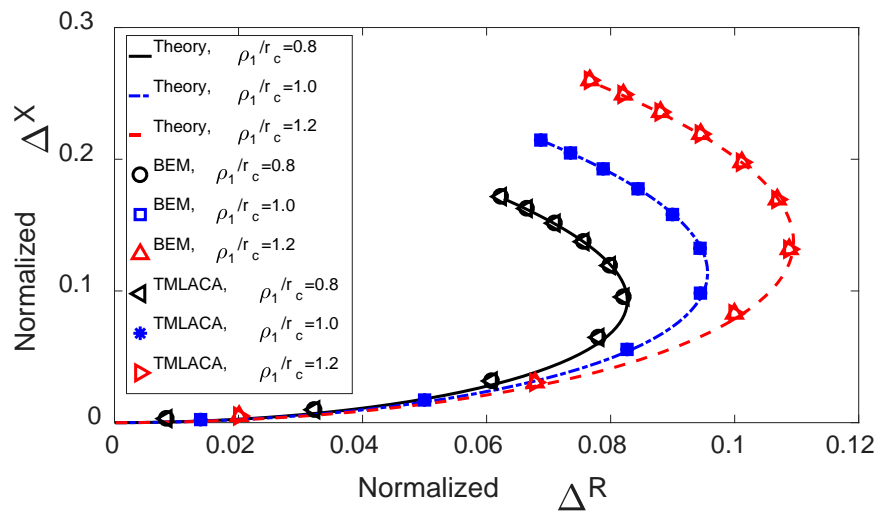
**Fig. 7.** Single turn coil above conducting sphere.

**TABLE IV**  
 SINGLE TURN COIL IS ABOVE THE CONDUCTING SPHERE

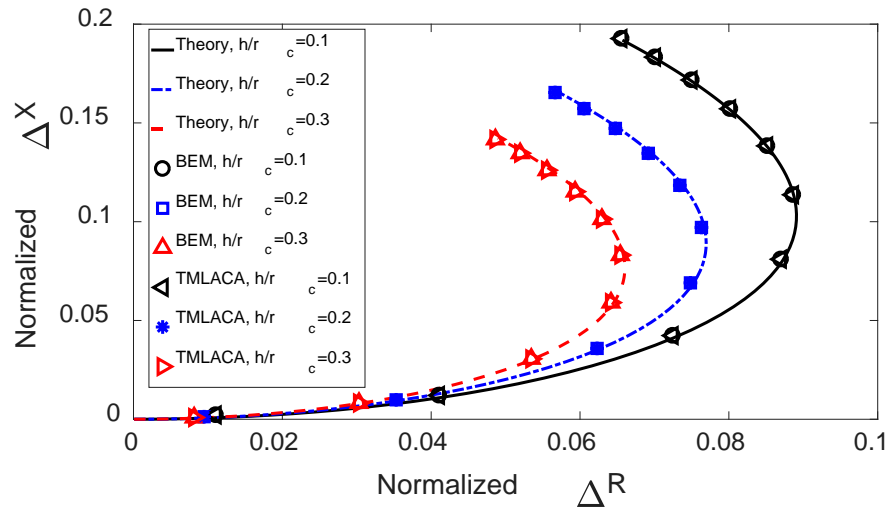
	IMPEDANCE CHANGE ( $\text{m}\Omega$ )	MEMORY REQUIREMENT ( $\text{MB}$ )	CPU TIME PER ITERATION (s)
Analytical Method [35]	$0.5216 + 1.614i$	n/a	n/a
BEM	$0.5190 + 1.620i$	2799	0.48
ACA	$0.5190 + 1.620i$	1180	0.178
MLACA	$0.5190 + 1.620i$	980	0.142
TMLACA	$0.5205 + 1.621i$	624	0.085

From Table IV, the relative differences of impedance change between the numerical and the analytical results are smaller than 1%. The MLACA based BEM needs 35% memory of the BEM and uses 17% less memory than the ACA based BEM. For the memory cost of the far block interactions and the CPU time per iteration, the TMLACA based BEM uses 74% and 40% less than the MLACA based BEM.

The comparison of normalized impedance changes against  $\beta$  for different ratios of  $\rho_1/r_c$  and  $h/r_c$  calculated by the analytical method [35], the BEM and the TMLACA based BEM are shown in Fig. 8. The points on the curves correspond to  $\beta=1,\dots,10$ , where the lowest point on each curve corresponds to  $\beta=10$ . The relative differences are smaller than 1% of these three methods. Again, the results show the good agreements.



(a)



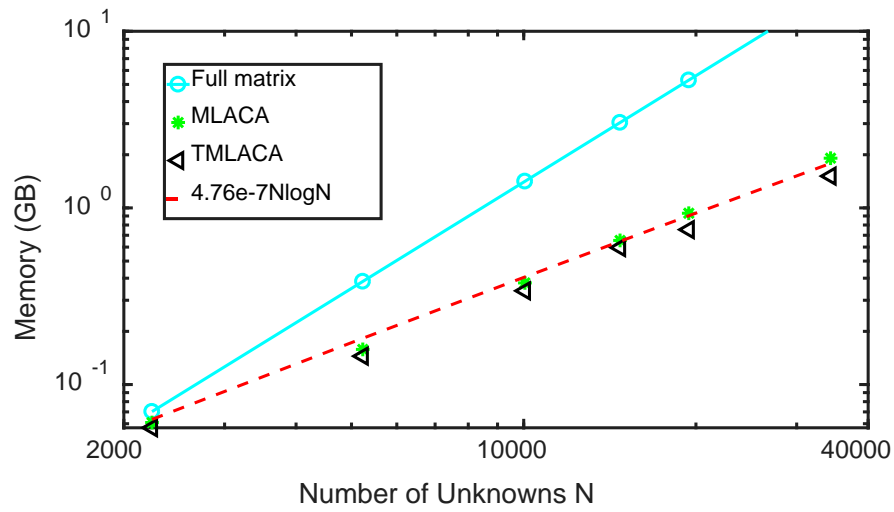
(b)

**Fig. 8.** (a) Comparison of normalized impedance changes against  $\beta$  for three values of  $\rho_1/r_c$  with  $h/r_c = 0.1$ . (b) Comparison of normalized impedance changes against  $\beta$  for three values of  $h/r_c$  with  $\rho_1/r_c = 0.1$ . The results are calculated by the analytical method [35], the BEM and the TMLACA based BEM with relative permeability  $\mu_r = 1$ .

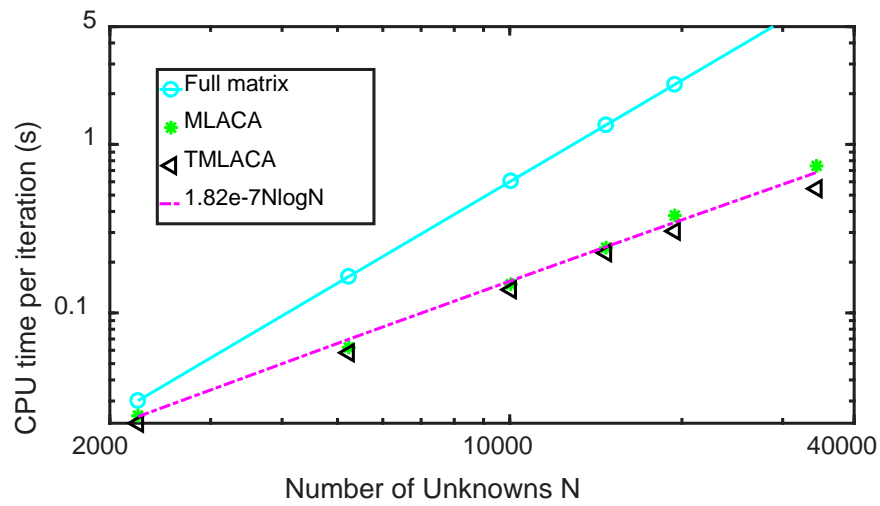
## 4.2 Complexity

Having demonstrated the accuracy of the proposed method, the performance of the MLACA based BEM and the TMLACA based BEM will be presented in this section. We select the case with the coil inside the borehole which does not have the naturally null matrices issue to show the complexity of the MLACA. The frequency is 5 kHz and the skin depth is 7.8 mm. The infinite long borehole is truncated with the height around 62 mm and the edge size of the triangular mesh varies from 0.1 to 0.5 times the skin depth. Based on the criteria, we adaptively apply 1, 2 and 3 stages MLACA to different operators at different levels with the tolerance  $\varepsilon = 10^{-2}$ . The threshold value  $\Delta_1$  of the TMLACA is  $10^{-4}$ . All the results are achieved with the relative differences of impedance changes between the full matrix method, the MLACA based BEM and the TMLACA based BEM are smaller than 1%. The complexity of memory requirement for all the near, diagonal and near far block interactions and the CPU time are shown in Fig. 9 (a) and (b) respectively.

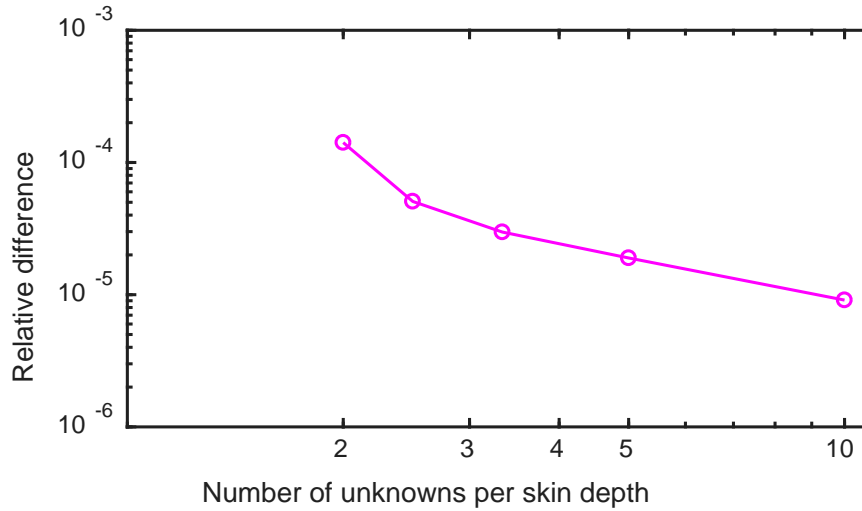
The accuracy relates to the number of unknowns per skin depth is shown in Fig. 9 (c).



(a)



(b)



(c)

**Fig. 9.** Performance of the MLACA and the TMLACA based BEM. (a) Memory requirement. (b) CPU time per iteration. (c) Relative differences of impedance changes against the number of unknowns per skin depth. Fixed geometry, decrease the mesh size to get more number of unknowns. Comparison between the full matrix (BEM), the MLACA based BEM and the TMLACA based BEM for the case of the coil carrying a current with frequency at 5 kHz inside the borehole. The number of unknowns is approximately from 2,000 to 50,000.

In Fig. 9, we plot the memory requirement and CPU time per iteration for the full matrix method (BEM), the MLACA based BEM and the TMLACA based BEM for the case of the coil inside the borehole with the number of unknowns approximately from 2,000 to 50,000. For the electrically small problems, the complexity of memory requirement and CPU time for full matrix method is  $O(N^2)$  while that for the MLACA based BEM is  $O(N \log N)$  which agrees well with [22]. The rule, that at least 2 unknowns per skin depth, leads to good accuracy. The more number of unknowns per skin depth is used, the more accurate results can be achieved.

It is shown in the figure that the MLACA based BEM only needs an average 32% of memory

requirement and 36% of CPU time of the BEM. Also, the MLACA based BEM uses average 21% memory and 16% CPU time less than the ACA based BEM. For the cost of the far block interactions, the TMLACA based BEM uses average 21% less memory than the MLACA based BEM, and average 63% less memory than the ACA based BEM. For the overall performance, the TMLACA based BEM uses average 12% memory, 12% matrix filling time and 13% CPU time per iteration less than the MLACA based BEM, and average 33% in memory, 31% matrix filling time and 30% CPU time per iteration less than the ACA based BEM. Among all these methods, the TMLACA based BEM requires the least memory requirement and CPU time cost which demonstrates the efficiency of it.

## 5. Conclusions

In this article, the multilevel adaptive cross approximation algorithm with the truncated integral kernels (TMLACA) is proposed to accelerate the BEM for 3D arbitrary shaped eddy current NDE problems. We found the criteria for different operators to optimize the performance of TMLACA. By adaptively applying the multi-stage (level) algorithm based on the criteria determined, the TMLACA based BEM can improve the efficiency while keeping the accuracy as compared with the traditional MLACA based BEM for eddy current problems with large solution domain. Several practical 3D arbitrary shaped ECT cases are analyzed. The numerical results calculated by the TMLACA based BEM are compared with the BEM, the ACA based BEM, the MLACA based BEM, the analytical method, the semi-analytical method and the experiments. Both good accuracy and efficiency of the TMLACA are observed for all cases. The proposed high performance method can be applied as the fast predictions for the eddy current NDE problems.

## Acknowledgment

This work is supported in part by the IU Program of the Center for Nondestructive Evaluation at Iowa State University, by China Scholarship Council, by National Natural Science Foundation of China (61601185) and by Natural Science Foundation of Jiangxi Province (20171ACB21040). The authors are

grateful to Dr. M. Yang for providing BEM codes and Dr. T. Wu for providing the semi-analytical results for the coil in the borehole.

## References

- [1] C.V. Dodd and W.E. Deeds, "Analytical solutions to eddy-current probe-coil problems," *J. Appl. Phys.*, vol. 39, pp. 2829-2838, May 1968.
- [2] T.P. Theodoulidis and J.R. Bowler, "Eddy current coil interaction with a right-angled conductive wedge," *Proceedings of Royal Society*, vol. 461, pp. 3123-3139, Aug. 2005.
- [3] T. Kincaid and M. Chari, "The application of finite element method analysis to eddy current nondestructive evaluation," *IEEE Trans. Mag.*, vol.15, no. 6, pp. 1956-1960, Nov. 1979.
- [4] W.C. Chew, M.S. Tong, and B. Hu, *Integral equation methods for electromagnetic and elastic waves*. London: Morgan & Claypool, 2008.
- [5] T.P. Theodoulidis, N. Poulakis, and A. Dragogias, "Rapid computation of eddy current signals from narrow cracks," *NDT&E International*, vol. 43, no.1, pp. 13-19, Aug. 2009.
- [6] J.R. Bowler, L.D. Sabbagh, and H.A. Sabbagh, "A theoretical and computational model of eddy-current probes incorporating volume integral and conjugate gradient methods," *IEEE Trans. Mag.*, vol. 25, no. 3, pp. 2650-2664, May 1989.
- [7] J.R. Bowler. "Eddy-current interaction with an ideal crack. i. the forward problem," *J. Appl. Phys.*, vol. 75, no. 12, pp. 8128-8137, Feb. 1994.
- [8] R. Miorelli, C. Reboud, T.P. Theodoulidis, J. Martinos, N. Poulakis, and D. Lesselier, "Coupled approach VIM-BEM for efficient modeling of ECT signal due to narrow cracks and volumetric flaws in planar layered media," *NDT&E International*, vol. 62, pp. 178-183, Jan. 2014.
- [9] J.M. Song, C.C. Lu, and W.C. Chew, "Multilevel fast multipole algorithm for electromagnetic scattering by large complex objects," *IEEE Trans. Antennas Propag.*, vol. 45, no. 10, pp. 1488-1493, Oct. 1997.
- [10] W.W. Chai and D. Jiao, "Direct matrix solution of linear complexity for surface integral-equation-based impedance extraction of complicated 3-D structures," *Proceedings of the IEEE*, vol. 101, no. 2, pp. 372-388, Feb. 2013.
- [11] L. Tsang, Q. Li, P. Xu, D. Chen, and V. Jandhyala, "Wave scattering with UV multilevel partitioning method: 2. Three-dimensional problem of nonpenetrable surface scattering," *Radio Sci.*, vol. 39, RS5011, Oct. 2004.

- [12] W.W. Chai and D. Jiao, "An  $H^2$ -matrix-based integral-equation solver of reduced complexity and controlled accuracy for solving electrodynamic problems," *IEEE Trans. Antennas Propag.*, vol. 57, pp. 3147-3159, Oct. 2009.
- [13] E. Michielssen and A. Boag, "A multilevel matrix decomposition algorithm for analyzing scattering from large structures," *IEEE Trans. Antennas Propag.*, vol. 44, no. 8, pp. 1086-1093, Aug. 1996.
- [14] M. Bebendorf, "Approximation of boundary element matrices," *Numer. Math.*, vol. 86, no. 4, pp. 565-589, Oct. 2000.
- [15] J. Smajic, Z. Andjelic, and M. Bebendorf, "Fast BEM for eddy-current problems using H-matrices and adaptive cross approximation," *IEEE Trans. Mag.*, vol. 43, pp. 1269-1272, Apr. 2007.
- [16] D. Pusch et al., "Comparison between BEM and classical FEM for a 3D low-frequency eddy-current analysis," *IEEE Trans. on Mag.*, vol. 46, no. 8, pp. 2919-2922, Aug. 2010.
- [17] P. Alotto et al., "Sparsification of BEM matrices for large-scale eddy current problems," *IEEE Trans. on Mag.*, vol. 52, no. 3, pp. 7203204, Mar. 2016.
- [18] G. Rubinacci et al., "A fast technique applied to the analysis of Resistive Wall Modes with 3D conducting structures," *J. Comput. Phys.*, vol. 228, no. 5, pp. 1562-1572, Mar. 2009.
- [19] K. Zhao, M.N. Vouvakis, and J.F. Lee, "The adaptive cross approximation algorithm for accelerated method of moments computations of EMC," *IEEE Trans. Electromagn. Compat.*, vol. 47, no. 4, pp. 763-773, Nov. 2005.
- [20] M. Bebendorf and S. Kunis. "Recompression techniques for adaptive cross approximation," *Journal of Integral Equations and Applications*, vol. 21, no. 3, pp. 331-357, Oct. 2009.
- [21] A. Heldring, J.M. Tamayo, C. Simon, E. Ubeda, and M. Rius, "Sparsified adaptive cross approximation algorithm for accelerated method of moments computations," *IEEE Trans. Antennas Propag.*, vol. 61, pp. 240-246, Jan. 2013.
- [22] J.M. Tamayo, A. Heldring, and J.M. Rius, "Multilevel adaptive cross approximation (MLACA)," *IEEE Trans. Antennas Propag.*, vol. 59, no. 12, pp. 4600-4608, Dec. 2011.
- [23] X.L. Chen, C.Q. Gu, J. Ding, Z. Li and Z. Niu, "Multilevel fast adaptive cross approximation algorithm with characteristic basis functions," *IEEE Trans. Antennas Propag.*, vol. 63, no. 9, pp. 3994-4002, Sep. 2015.
- [24] Z.N. Jiang, H. Chen, T. Wan, Y.M. Ouyang, X.G. Qiao and X.C. Lu, "Application of multilevel directional adaptive cross approximation technique for electromagnetic problems," *Engineering Analysis with Boundary Elements*, vol. 85, pp. 111-115, Dec. 2017.

- [25] S.M. Rao, D.R. Wilton, and A.W. Glisson, "Electromagnetic scattering by surfaces of arbitrary shape," *IEEE Trans. Antennas Propag.*, vol. 30, no. 3, pp. 409-428, May 1982.
- [26] Y. Bao, Z.W. Liu, and J.M. Song, "MACA algorithm to accelerate modeling of eddy current position sensor," *Applied Computational Electromagnetic Society Journal*, accepted.
- [27] Y. Bao, Z.W. Liu, and J.M. Song, "Adaptive cross approximation algorithm for accelerating BEM in eddy current nondestructive evaluation," *J. Nondestructive Evaluation*, vol. 37, no. 68, pp. 1-8, Dec. 2018.
- [28] J.A. Stratton, *Electromagnetic Theory*. New York, NY: McGraw-Hill, 1941.
- [29] M. Yang, *Efficient Method for Solving Boundary Integral Equation in Diffusive Scalar Problem and Eddy Current Nondestructive Evaluation*, Ph.D. dissertation, Iowa State Uni., Ames, IA, USA, 2010.
- [30] S. Börm and L. Grasedyck, "Hybrid cross approximation of integral operators," *Numer. Math.*, vol. 101, no. 2, pp. 221-249, Aug. 2005.
- [31] B.A. Auld and J.C. Moulder, "Review of advances in quantitative eddy current nondestructive evaluation," *J. Nondestructive Evaluation*, vol. 18, no. 1, pp. 3-36, March 1999.
- [32] T. Wu, *The Theory of Eddy Current Nondestructive Evaluation by Using the Volume Integral Equation Method*, Ph.D. dissertation, Iowa State Uni., Ames, IA, USA, 2016.
- [33] T. Wu and J.R. Bowler, "Eddy-current induction by a coil whose axis is perpendicular to that of a tube," *IEEE Trans. Mag.*, vol. 53, no. 7, pp. 1-9, July 2017.
- [34] J.R. Bowler and N. Bowler, *Eddy Current Nondestructive Evaluation*, EE 558 Notes, Ames, IA, USA, Sep. 2007.
- [35] M.Y. Antimorov, A.A. Kolyshkin, and R. Vaillancourt, *Mathematical models for eddy current testing*. Montreal, Canada: Les Publications CRM, 1997.